INTERNATIONAL JOURNAL OF OPTIMIZATION IN CIVIL ENGINEERING
Int. J. Optim. Civil Eng., 2026; 16(2):223-244

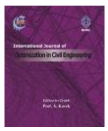

ENHANCING THE SEISMIC PERFORMANCE OF STEEL MOMENT FRAME STRUCTURES THROUGH THE OPTIMAL TUNING OF A PASSIVE INERTER-TUNED MASS DAMPER

R. Kamgar[1*, †] and S. Rostami[2]
[1]*Department of Civil Engineering, Shahrekord University, Shahrekord, Iran*
[2]*Department of Civil Engineering, Technical and Vocational University (TVU), Tehran, Iran*

ABSTRACT

A new type of seismic control device is introduced—the elastoplastic inerter-tuned mass damper—which omits the conventional viscous damping element and instead incorporates stiffness with elastoplastic behavior. The key objective is to benchmark its earthquake performance against alternative vibration mitigation strategies, including the standard tuned mass damper, the elastoplastic tuned mass damper, and the inerter-tuned mass damper. For each configuration, the design variables are optimized by minimizing the Park–Ang damage index, thereby maximizing the structure's seismic resilience. A nine-story moment-resisting frame is employed and is modeled with the OpenSees software nonlinearly. Simulation results reveal that the proposed elastoplastic inerter-tuned mass damper surpasses all other examined systems. Specifically, it delivers up to a 38% drop in the global damage index and a 50% damage reduction in the lower stories.

Keywords: Inerter tuned mass damper; Park-Ang damage index; Optimization; Drift ratio.

Received: 20 February 2026; Accepted: 28 April 2026

1. INTRODUCTION

Earthquakes have repeatedly inflicted severe human and economic losses throughout history, primarily through the collapse of buildings and high-rise structures. Over recent decades, the implementation of damping devices has emerged as a highly effective approach for mitigating vibration responses in structures subjected to seismic excitations. A substantial body of research confirms that such equipment plays a critical role in safeguarding structures against

[*]Corresponding author: Department of Civil Engineering, Shahrekord University, Shahrekord, Iran
[†]E-mail address: kamgar@sku.ac.ir (R. Kamgar)

earthquake-induced damage. Consequently, the parametric study and optimal tuning of damper characteristics constitute essential steps in seismic vibration control strategies.

As engineering knowledge has progressed and dynamic load characterization has improved in recent years, the analysis of structures under combined gravitational and time-varying loads has become increasingly intricate, presenting new performance challenges. To address these disturbances, the adoption of control systems in the construction sector has become unavoidable. In response, the investigation and development of vibration control techniques for natural hazards—particularly earthquakes and wind—have assumed a central position within structural engineering.

Currently, structural vibration control methodologies are generally classified into three principal groups (i.e., Active control systems, Semi-active control systems, and Passive control systems). Among the most prevalent passive control devices is the Tuned Mass Damper (TMD). A TMD typically comprises a mass, a spring, and a damping element attached to the structure; its effectiveness is strongly governed by the careful selection of its design parameters.

In the current study, inspired by Smith's 2002 concept, a mass-amplification mechanism known as an "inerter" has been integrated into the conventional TMD architecture. In this modified configuration, the viscous damper is omitted, and linear stiffness is replaced by elastoplastic stiffness to enhance performance relative to the classical TMD. This new arrangement is designated as the Elastoplastic Inerter Tuned Mass Damper (PTMDI), which capitalizes on the inertance effect to amplify apparent mass.

Achieving superior vibration control with this system necessitates an optimal design of its parameters. The significance of such optimization is profound, as a detailed examination can substantially contribute to the advancement of structural dynamics and earthquake engineering knowledge.

Across civil and mechanical engineering, structural vibration control can be realized through diverse strategies—modifying stiffness, mass, or damping; altering the form or geometry; or employing active or passive counter-forces. The inaugural concept of a tuned mass damper was proposed by Frahm in 1909 to attenuate wave-induced oscillations in naval vessels. Later, in 1928, Ormondroyd and Hartog developed the first theoretical framework for damper performance, accounting for structural damping while idealizing the damper itself as undamped. Their findings highlighted that incorporating damping within the device itself significantly enhances control effectiveness [1]. Subsequently, in 1946, Brock introduced an optimal methodology for selecting the damping ratio in TMD systems—a milestone that shaped modern TMD design. Since that time, the TMD has been investigated in its contemporary form [2].

More recently, tuned mass dampers have attracted widespread research interest as one of the most effective means of reducing earthquake-induced structural vibrations [3-6]. Numerous studies substantiate their protective capability against seismic damage. Following the foundational contributions of Den Hartog and Ormondroyd [1], diverse optimal design pathways have been developed to tailor TMDs for earthquake excitation [7].

Among the various design methodologies, the fixed-point theory remains one of the most frequently employed [8]. It provides closed-form analytical solutions for determining optimal TMD parameters, facilitating reliable tuning of the device [9].

Early TMD models comprised a mass, a spring, and a viscous damper attached to the structure, operating through relative motion to dissipate vibrational energy. From a practical viewpoint, increasing the attached mass can improve TMD performance, provided that structural and architectural constraints allow such augmentation. Some researchers have recommended installing large-mass TMDs at upper floors or over the top few stories, often in conjunction with seismic isolation systems [10].

Identifying suitable installation locations and precisely determining TMD parameters—mass, stiffness, and damping—have been recurrent themes in related investigations [11-12].

A new generation of lighter-weight TMDs is currently under development, aiming to match or exceed the performance of classical designs. These systems incorporate the inerter mechanism, first introduced by Smith in 2002 [13]. Originally devised for automotive suspension, the inerter generates a resistive force proportional to the relative acceleration across its terminals, effectively mimicking a much larger inertial mass. This characteristic renders it an attractive low-mass alternative to conventional TMDs. Multiple inerter variants have since been developed [14].

In structural engineering, the overarching goal of vibration control is to mitigate dynamic responses under lateral loads—wind and earthquakes. TMDs represent one effective solution, comprising a mass, a spring of prescribed stiffness, and a damper. As passive devices, they operate most efficiently when their natural frequency is tuned to the first mode of the primary structure, ideally at resonance, enabling energy transfer and dissipation through damping [15].

The efficacy of a TMD hinges on the accurate calibration of its mass, stiffness, and damping for the specific structure and seismic conditions. This calibration constitutes a formidable engineering challenge [16], spurring extensive research into optimal parameter determination under seismic loading. Various optimization algorithms have been developed to address such problems [17-19].

Shayesteh Bilondi *et al*. [20] suggested optimizing TMDs based on hysteretic energy reduction. Although useful, this approach is incomplete, as the damage index—which integrates displacement ductility and hysteretic energy—offers a more comprehensive performance metric. Minimizing this index via optimization can effectively curtail structural damage during and after major earthquakes.

Other studies have expanded upon these ideas. Baker and Jangid [21] optimized TMD parameters to suppress undesirable vibrations in SDOF systems under external excitations. Bekdas and Nigdeli [22] employed the harmony search algorithm for parameter optimization. Recently, Lu *et al*. [23] applied differential evolution to derive optimal TMD parameters for nonlinear building responses.

Past research has consistently underscored that increasing the attached mass enhances TMD effectiveness; however, this also imposes a practical constraint, as heavier masses may be difficult to accommodate.

Numerical integration is required to solve the dynamic equations of motion when optimizing TMD parameters. In this study, the Newmark method is adopted for this purpose. Despite notable progress in TMD design—especially those incorporating inerters for seismic control—comprehensive investigations remain limited. Studies on Viscous Mass Dampers (VMDs), Tuned Viscous Mass Dampers (TVMDs), and Inerter-based Dampers (TIDs) have largely been grounded in frequency-domain analyses [24-25].

TMD performance depends critically on precise tuning [22] and is influenced by earthquake characteristics—distance, frequency content, and duration. While TMDs exhibit acceptable performance under wind [26], their effectiveness varies for seismic excitations; they may be beneficial for long-duration, moderate-amplitude motions, but are less recommended for short, intense records [27-28].

Simultaneously, the development of lightweight inerters continues, with Smith's 2002 invention serving as the foundation [13]. Originally for automotive applications, the inerter's ability to generate a force proportional to relative acceleration has established it as a promising substitute for bulky masses. Many inerter configurations are now available [29].

The Inerter Tuned Mass Damper (TMDI) was first analytically formulated by Marian and Giaralis using stochastic input to minimize structural response [30]. Brzeski *et al*. explored adjustable-inertia designs for TMDs [31]. Other studies have examined inerter-damper configurations under seismic loads, confirming their response-reduction effectiveness [24, 31-32].

Elastoplastic Tuned Mass Dampers (PTMDs) have also drawn attention recently. Jaiswal *et al*. introduced this variant, demonstrating improved performance over classical TMDs, primarily by eliminating the damper and incorporating nonlinear stiffness [33].

Damage assessment under seismic loading has emerged as a central theme in structural and earthquake engineering. Damage indices are broadly classified as qualitative or quantitative; numerous criteria have been proposed, including the Park-Ang index, ductility ratio, secant stiffness, cumulative dissipated energy, and the Venzian-Benan index.

In this study, following the introduction of the novel Elastoplastic Inerter Tuned Mass Damper (PTMDI), the optimization of its parameters is performed using meta-heuristic algorithms. The primary objective is to minimize the Park-Ang damage index, thereby enhancing the seismic performance of the structure and reducing its vulnerability to earthquake-induced damage.

2. META-HEURISTIC ALGORITHM ADOPTED FOR THE OPTIMIZATION PROBLEM

Over recent years, a diverse array of techniques has emerged for the optimal sizing and tuning of structural parameters. These techniques are broadly divisible into two principal categories: deterministic strategies and probabilistic strategies. Within the former, computer-based computational procedures—often relying on gradient-sensitive optimization schemes—are extensively employed. Such approaches operate by differentiating the objective function and enforcing the relevant design constraints to derive optimal values for the structural variables.

Conversely, meta-heuristic and exploratory algorithms, which draw inspiration from natural phenomena, collective behaviors, and biological processes, belong to the probabilistic family. By emulating evolutionary dynamics, swarm intelligence, or organismal interactions, these algorithms have proven to be robust tools for tackling challenging design problems characterized by complexity and nonlinearity.

A pivotal element in any successful optimization endeavor is the judicious formulation of the objective function. This function serves as the guiding criterion that steers the search process, typically encapsulating a critical performance indicator of the problem at hand.

Consequently, careful attention to the definition and selection of an appropriate objective function is essential for achieving optimal outcomes.

2.1. Harris Hawks Optimization algorithm [34]

Figure 1 provides a visual depiction of the sequential stages comprising the Harris Hawks optimization algorithm. A detailed, step-by-step discussion of each of these phases is presented in the subsequent sections.

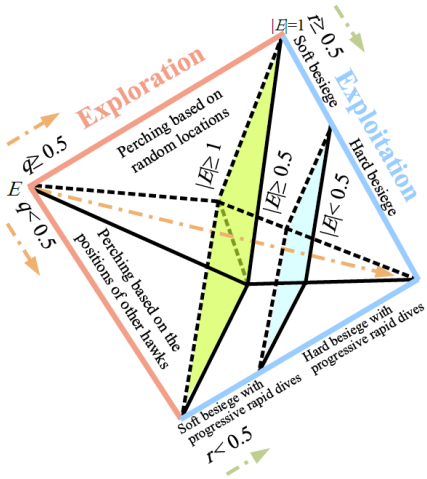

Figure 1: Different steps of the Harris Hawks optimization algorithm [34].

2.1.1. Exploration Stage

At the outset of the Harris Hawks algorithm, an initial population of hawks is distributed stochastically across the solution domain. Employing two principal tactics, these raptors strategically conceal themselves and commence the detection of their target. These twin strategies underpin the algorithm's subsequent searching mechanism and exert a critical influence on steering the overall optimization trajectory [34].

$$X(t+1)=\begin{cases} X_{rand}(t)-r_1\left|X_{rand}(t)-2r_2X(t)\right| & q\geq 0.5 \\ (X_{rabbit}(t)-X_m(t))-r_s(LB+r_4(UB-LB)) & q<0.5 \end{cases} \tag{1}$$

As shown in Equation (1), $X(t+1)$ is the position vector of the hawk at iteration t, $X_{rabbit}(t)$ is the position of the prey (rabbit), $X(t)$ is the current position vector of the hawks, r_1, r_2, r_s, and q are random numbers in the range [0, 1] that are updated at each iteration. LB and UB denote the lower and upper bounds of the variables, $X_{rand}(t)$ is a randomly selected hawk from the current population, and $X_m(t)$ is the mean position of the hawks. The mean position of the hawks from the current population is obtained using the following equation [34]:

$$X_m(t) = \frac{1}{N}\sum_{i=1}^{N} X_i(t) \tag{2}$$

As shown in Equation (2), $X_i(t)$ is the position of each hawk at iteration t, and N represents the total number of hawks [34].

2.1.2. Transition from Exploration to Exploitation Phase

To model this phase, the energy of the prey (rabbit) is expressed as follows [34]:

$$E = 2E_0(1-\frac{t}{T}) \tag{3}$$

The prey's (rabbit's) escape energy, denoted as E, is given by Equation (3), where T is the total iteration count, and E_0 is the initial energy. Additionally, the temporal evolution of E is visualized in Figure 2 [34].

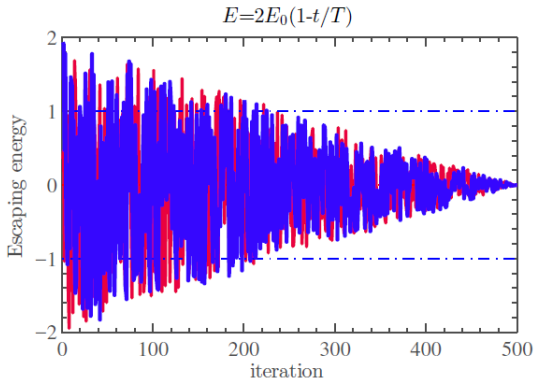

Figure 2: Behavior of E over two runs and 500 iterations [34].

2.1.3. Exploitation Phase

2.1.3.1. Soft Encirclement

This behavior is modeled using the following rules [34]:

$$X(t+1) = \Delta X(t) - E\left|JX_{rabbit}(t) - X(t)\right| \qquad J = 2(1-r_s) \tag{4}$$

$$\Delta X(t) = X_{rabbit}(t) - X(t) \tag{5}$$

As defined in Equations (4) and (5), the term $\Delta X(t)$ denotes the vectorial difference between the prey's current position and the hawk's location at iteration t. The parameter r_s is a uniformly distributed random number within the interval [0, 1], while $J = 2(1-r_s)$ represents the prey's stochastic jumping energy during evasion. To mimic the erratic nature of the prey's escape, the value of J is randomly updated at each iteration [34].

2.1.3.2. Hard Encircling

In this scenario, the position vectors are updated according to the following relation [35]:

$$X(t+1) = X_{rabbit}(t) - E\left|\Delta X(t)\right| \tag{6}$$

A simple example of this phase, along with a hawk, is shown in Figure 3 [34-35]:

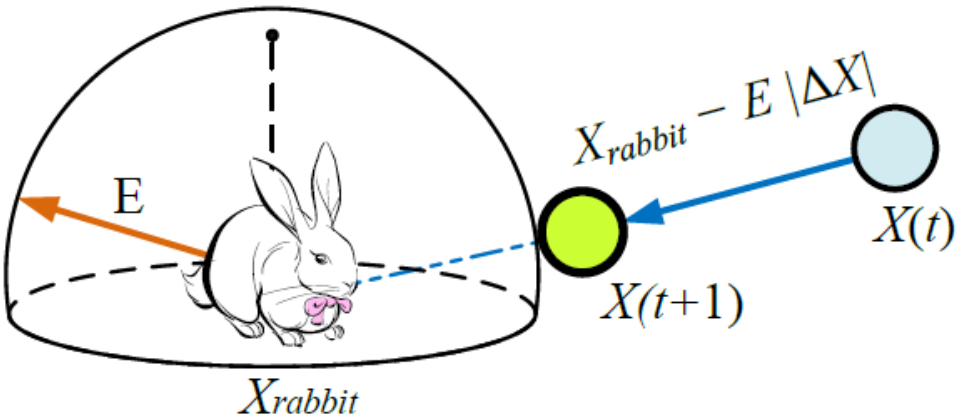

Figure 3: Behavior of *E* over two runs and 500 iterations [34-35].

3. SEISMIC CONTROL STRATEGIES FOR STRUCTURAL SYSTEMS

3.1. Structural Configuration Incorporating PTMDI

In the conventional tuned mass damper (TMD), the relationship between applied force and resulting deformation is presumed to remain linear across all loading regimes. By contrast, the elastoplastic inerter-based tuned mass damper introduces a yielding threshold at the characteristic deformation u_y, beyond which the force-deformation response deviates from linearity.

In the elastoplastic model, the yield stress is taken as equal for both positive and negative deformation directions. Unloading from a state of peak deformation follows a trajectory that runs parallel to the initial elastic segment. Likewise, upon reloading from a state of minimum deformation, the loading curve again parallels the initial elastic branch.

Within this framework, the resistive force generated by the system at any instant t is a function of its prior deformation history—specifically, it hinges on whether the deformation magnitude is currently increasing or decreasing. For the PTMDI configuration, the normalized yield stress relation is expressed as follows [36]:

$$\bar{f}_y = \frac{f_y}{f_0} = \frac{u_y}{u_0} \tag{7}$$

As defined in Equation (7), the parameters f_0 and u_0 correspond to the peak resistive force and the maximum deformation exhibited by a linearly elastic system, respectively. Stated differently, f_0 denotes the threshold resistance necessary to preserve structural stability during a seismic event. Additionally, u_y signifies the deformation at yield, while f_y represents the corresponding yield force. Also, the maximum deformation is denoted as u_m [36].

Figure 4 depicts a single-degree-of-freedom (SDOF) structure equipped with an elastoplastic inerter-based tuned mass damper (PTMDI), subjected to ground acceleration $\ddot{x}_g(t)$. The primary structure is characterized by its mass, stiffness, and damping properties. A supplementary device—featuring nonlinear (elastoplastic) mass and stiffness behavior—is attached to the upper portion of the system. This configuration is specifically designed to improve seismic performance and mitigate the dynamic response of the structure.

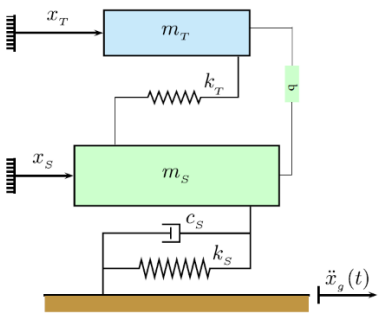

Figure 4: Schematic representation of a single-degree-of-freedom (SDOF) structural system equipped with a PTMDI device positioned at the top, subjected to seismic ground motion excitation.

The fundamental concept underlying inerter devices was originally proposed by Smith [13]. An ideal inerter is characterized as a linear two-terminal mechanical element of negligible mass, capable of unrestrained motion. Its most distinctive attribute lies in the generation of a resisting force F, the magnitude of which is directly proportional to the relative acceleration between its two terminals. The corresponding mathematical expression for the force developed across the two terminals of the inerter is given as:

$$F = b(\ddot{u}_1 + \ddot{u}_2) \tag{8}$$

As expressed in Equation (8), the quantities $\ddot{u}_1$ and $\ddot{u}_2$ correspond to the accelerations at the two terminals of the inerter device. Within this equation, the parameter b serves as the proportionality factor, formally designated as "inertance," and is quantified in units of mass [13].

A particularly noteworthy aspect of the inerter's operation is its ability to substantially amplify the effective mass of the damping system, such that its inertial contribution far exceeds its actual physical mass. This distinctive behavior has been corroborated through experimental investigations on early-stage inerter prototypes, which were specifically engineered to transform translational kinetic motion into rotational kinetic energy.

The governing expression for the inertance coefficient—or proportionality constant—is presented below [13]:

$$b = m_f \frac{\gamma_f^2}{\gamma_{pr}^2} \left(\prod_{q=1}^{n} \frac{r_q^2}{pr_q^2} \right) \tag{9}$$

As defined in Equation (9), the quantities denoted by m_f and γ_f correspond, respectively, to the mass and radius of the flywheel. Furthermore, γ_{pr} represents the rotational radius of the pinion that is mechanically coupled to the flywheel, while $\frac{r_q}{pr_q}$ indicates the gear ratio pertaining to the q stage of the power transmission system [13].

A key point to emphasize is that through proper tuning of the gear ratios, the apparent inertial mass can be substantially increased. This enhanced inertance enables the device to behave as if it had a mass far exceeding its physical counterpart, thereby contributing significantly to improved dynamic response. Viewed from this angle, the ideal inerter functions as an amplifier of inertia, since it mimics an inertial element when linked to either of its terminals. In the current study, these distinctive properties are harnessed within an elastoplastic inerter tuned mass damper (PTMDI) to boost the efficacy of traditional vibration mitigation systems.

The frequency ratio of the PTMDI system is defined as follows:

$$\omega_{PTMDI} = \frac{\sqrt{\frac{k_T}{(m_T + b)}}}{\omega_s}, \tag{10}$$

In Equation (10), ω_s denotes the natural frequency of the primary structure. Also, k_T and m_T show the stiffness and mass of the PTMDI system, respectively.

4. ASSESSMENT OF PERFORMANCE LEVELS

The FEMA-356 guidelines [37] establish distinct structural performance thresholds based on interstory drift ratios, as summarized in Table 1. According to these provisions, when the interstory drift remains below 1%, structural members experience only minor damage, corresponding to the "Immediate Occupancy" (IO) performance level.

Should the drift ratio reach 2%, both structural and non-structural components sustain considerable damage, defining the "Life Safety" (LS) performance level. At a drift ratio of 4%, the structure approaches incipient collapse, which is designated as the "Collapse Prevention" (CP) level.

Beyond the 4% drift limit, the structure is considered to have reached the "Collapse" (C) state, indicating total failure and the complete loss of structural integrity.

Table 1: Performance level classifications per FEMA-356 [37] for steel moment-resisting frames.

Performance level	IO	LS	CP	C
Story drift (%)	1	2	4	>4

5. DAMAGE INDEX

In the context of structural performance assessment, a critical step involves the thorough examination of damage sustained by individual structural members, which ultimately contributes to the overall damage estimation of the system. Over recent decades, numerous damage indices have been proposed by various researchers, each grounded in distinct evaluation criteria.

The damage index adopted in this study is formulated based on the energy dissipated by the structure and its ductility capacity. Among the most widely recognized measures is the Park-Ang damage index, which incorporates a linear combination of peak deformation and hysteretic energy dissipation observed during the loading history [38]. This index facilitates a more holistic evaluation of the nonlinear structural response under extreme loading events.

5.1. Park-Ang Damage Index

This section presents the required formulations for computing the damage index at the member level, the story level, and the overall structural level, employing the modified version of the Park-Ang damage index. This index is a well-established tool for assessing structural vulnerability under severe loadings, as it accounts for both maximum deformations and the cumulative hysteretic energy dissipated throughout the loading process.
The original expression for the Park-Ang damage index is given as [38]:

$$DI_{PA} = \frac{\delta_m}{\delta_u} + \frac{\beta}{Q_y \delta_u} \int dE \tag{11}$$

As expressed in Equation (11), the relevant parameters consist of the deformation experienced by the member under seismic acceleration δ_m, the ultimate deformation capacity of the member under monotonic loading δ_u, and β an experimentally derived empirical coefficient. For steel members, this coefficient has been established as 0.025 [39]. In addition, the formulation incorporates the yield stress of the member Q_y and the hysteretic energy dissipated (E), both of which are critical factors in damage quantification.

The Park-Ang damage index was subsequently refined by Kunnath and his colleagues, who reformulated it in terms of member rotation. This modified version serves as the foundation for the damage assessment procedure adopted in the current investigation [40], permitting a more refined characterization of the nonlinear response of structural components.

$$DI_{PA} = \frac{\theta_m - \theta_y}{\theta_u - \theta_y} + \frac{\beta}{M_y \theta_u} \int dE \tag{12}$$

Equation (12) defines the member-level parameters as follows: θ_m is the maximum end rotation attained by the member; θ_u denotes the ultimate rotational capacity; θ_y corresponds to the rotation at yielding; and M_y represents the yield moment of the cross-section.

The damage index for the entire structural system is subsequently evaluated using the expression given in Equation (13). In this formulation, λ_i and E_{h_i} denote the energy-weighting coefficients and the cumulative dissipated energy associated with the jth story or the ith member, respectively [41].

$$DI_{Storey} = \sum (\lambda_i)_{component} (DI_i)_{component} \; ; \quad (\lambda_i)_{component} = \left(\frac{E_{h_i}}{\sum E_{h_i}} \right)_{component}$$
$$DI_{Overall} = \sum (\lambda_j)_{Storey} (DI_j)_{Storey} \; ; \quad (\lambda_j)_{Storey} = \left(\frac{E_{h_j}}{\sum E_{h_j}} \right)_{Storey} \tag{13}$$

6. COMPARATIVE ASSESSMENT OF PTMDI, PTMD, TMDI, AND TMD IN REDUCING THE PARK-ANG DAMAGE INDEX

This section evaluates the practical benefits of the proposed Elastoplastic Inerter Tuned Mass Damper (PTMDI) by benchmarking its performance against three alternative configurations: the conventional Tuned Mass Damper (TMD), the Inerter-based Tuned Mass Damper (TMDI), and the Elastoplastic Tuned Mass Damper (PTMD). All comparisons are carried out within the framework of passive vibration control applied to structures exhibiting nonlinear behavior.

The central hypothesis of this investigation is that omitting the viscous damper in the PTMDI—while introducing nonlinear stiffness in its place and simultaneously harnessing the inertial amplification provided by the inerter—can substantially reduce the structural damage index. A key advantage of the PTMDI lies in its capacity to amplify inertance without necessitating a corresponding increase in the physical mass attached to the system, thereby offering improved performance relative to its counterparts.

To enable a rigorous comparison, a nine-story steel frame was simulated in the OpenSees environment, equipped successively with PTMDI, TMD, TMDI, and PTMD devices. The numerical model incorporated material nonlinearity through concentrated plasticity at the connection regions. Dynamic excitation was provided by an artificial ground motion record scaled to a peak ground acceleration of 0.8*g*.

The initial population for the Harris Hawks optimizer was selected after testing several candidates; the one yielding the most favorable convergence behavior was retained uniformly across all optimization runs. The ensuing numerical simulations demonstrated that the PTMDI system achieves a 38% reduction in the global damage index of the structure.

Overall, the comparative results confirm that the PTMDI—by virtue of eliminating the viscous element, substituting linear stiffness with an elastoplastic counterpart, and capitalizing on the inertance properties of the inerter—exhibits outstanding efficacy in lowering the

Park-Ang damage index. Notably, while the TMD and PTMD systems demand substantial mass ratios to attain satisfactory performance, the PTMDI delivers superior outcomes with a remarkably low mass ratio—approximately 0.01% of the structural mass. This finding introduces a novel perspective for designing lightweight yet highly efficient vibration control strategies.

6.1. Optimization Framework for the PTMDI System

Throughout history, structural collapse under seismic loading has remained one of the most critical threats to human life and built infrastructure. Excessive lateral displacements and floor accelerations are among the primary drivers of such failures. Contemporary engineering practice seeks to mitigate these adverse effects through vibration control technologies, thereby reducing the likelihood of collapse.

Among the various passive control alternatives, the PTMDI stands out as a promising solution. It consists of a mass and a nonlinear (elastoplastic) stiffness element. When the damper's natural frequency is tuned to the fundamental frequency of the primary structure, its motion becomes out-of-phase with the structural response, enabling significant energy dissipation through the nonlinear stiffness mechanism. This interaction leads to a marked attenuation of the dynamic response under seismic input.

The subsequent optimization effort focuses on the key parameters governing the PTMDI's performance—namely, the mass, the nonlinear stiffness, and the inertance level of the inerter. The objective is to minimize the Park-Ang damage index when the structure is subjected to the artificial earthquake record. The optimization procedure is outlined as follows:

$$
\begin{aligned}
&\text{Find} && m_T, k_T, F \\
&\text{Minimize:} && DI_{PA}(m_T, k_T, F) \\
&\text{Subjected to:} && \begin{cases} m_T^{\min} \le m_T \le m_T^{\max} \\ k_T^{\min} \le k_T \le k_T^{\max} \\ F^{\min} \le F \le F^{\max} \\ \max(\left|X_T(t) - X_{Roof}(t)\right| \le St_{\max} \\ DI_{PA}^{story} \le 0.3 \end{cases}
\end{aligned}
\tag{14}
$$

Equation (14) defines the permissible ranges for the PTMDI design variables: $m_T^{\min}$ and $m_T^{\max}$ specify the minimum and maximum allowable mass; $k_T^{\min}$ and $k_T^{\max}$ represent the corresponding bounds for the nonlinear stiffness; and $F^{\min}$ and $F^{\max}$ establish the lower and upper limits for the inertial force level generated by the inerter device connected to both the mass and the supporting floor. The relative displacement between the control system and its mounting floor—referred to as the stroke of the PTMDI—is constrained to a pre-defined maximum value, denoted as $St_{\max}=1\ (m)$, for this investigation. In the same equation, DI_{PA}^{story} corresponds to the Park-Ang damage index computed for each story of the structure. The

numerical bounds adopted for these parameters have been determined in accordance with reference [36], as summarized in Tables 3 through 7.

6.2. Optimization Formulation for the TMDI System

The optimization problem for the TMDI system is defined as follows:

$$\begin{aligned} &\text{Find} && m_T, k_T, c_T, F \\ &\text{Minimize:} && DI_{PA}(m_T, k_T, c_T, F) \\ &\text{Subjected to:} && \begin{cases} m_T^{\min} \le m_T \le m_T^{\max} \\ k_T^{\min} \le k_T \le k_T^{\max} \\ c_T^{\min} \le c_T \le c_T^{\max} \\ F^{\min} \le F \le F^{\max} \\ \max(\left|X_T(t) - X_{Roof}(t)\right| \le St_{\max} \\ DI_{PA}^{story} \le 0.3 \end{cases} \end{aligned} \tag{15}$$

Equation (15) defines the allowable ranges for the TMDI design variables: $m_T^{\min}$ and $m_T^{\max}$ establish the lower and upper bounds for the attached mass; $k_T^{\min}$ and $k_T^{\max}$ set the corresponding limits for the linear stiffness; $c_T^{\min}$ and $c_T^{\max}$ specify the permissible interval for the system damping; and finally, $F^{\min}$ and $F^{\max}$ delineate the bounds for the inertial force generated by the inerter device, which is coupled to both the mass and the supporting floor.

6.3. Optimization Formulation for the PTMD System

The optimization problem for the PTMD system is defined as follows:

$$\begin{aligned} &\text{Find} && m_T, k_T \\ &\text{Minimize:} && DI_{PA}(m_T, k_T) \\ &\text{Subjected to:} && \begin{cases} m_T^{\min} \le m_T \le m_T^{\max} \\ k_T^{\min} \le k_T \le k_T^{\max} \\ \max(\left|X_T(t) - X_{Roof}(t)\right| \le St_{\max} \\ DI_{PA}^{story} \le 0.3 \end{cases} \end{aligned} \tag{16}$$

Equation (16) defines the allowable ranges for the PTMD design variables: $m_T^{\min}$ and $m_T^{\max}$ establish the lower and upper bounds for the attached mass; $k_T^{\min}$ and $k_T^{\max}$ set the corresponding limits for the linear stiffness.

6.4. Optimization Formulation for the TMD System

The optimization problem for the TMD system is defined as follows:

$$\begin{aligned} &\text{Find} && m_T, k_T, c_T \\ &\text{Minimize:} && DI_{PA}(m_T, k_T, c_T) \\ &\text{Subjected to:} && \begin{cases} m_T^{\min} \le m_T \le m_T^{\max} \\ k_T^{\min} \le k_T \le k_T^{\max} \\ c_T^{\min} \le c_T \le c_T^{\max} \\ \max(\left|X_T(t) - X_{Roof}(t)\right| \le St_{\max} \\ DI_{PA}^{story} \le 0.3 \end{cases} \end{aligned} \tag{17}$$

Equation (17) defines the allowable ranges for the TMD design variables: $m_T^{\min}$ and $m_T^{\max}$ establish the lower and upper bounds for the attached mass; $k_T^{\min}$ and $k_T^{\max}$ set the corresponding limits for the linear stiffness; $c_T^{\min}$ and $c_T^{\max}$ specify the permissible interval for the system damping.

Table 2: Lower and upper bounds of the parameters considered in the optimization using the HHO algorithm.

Damping ratio [44]	Frequency ratio [43]	Mass ratio [44]	Inertance ratio [44]
$0.05 \le \zeta \le 2.5$	$0.01 \le \nu \le 10$	$0.002 \le \mu \le 0.02$	$0.0 \le \beta \le 1.0$

The parameters listed in Table 2 are generally expressed as follows:

$$\nu = \frac{\omega_0}{\omega_S},\ \zeta = \frac{c_0}{2m_0\omega_0},\ \mu = \frac{m_0}{m_S},\ \beta = \frac{b}{m_S} \tag{18}$$

As shown in Equation (18), ω_0, c_0, and m_0 represent the frequency, damping, and mass of the damper, respectively, while ω_S and m_S denote the frequency and mass of the main structure. Furthermore, the parameters ν, ξ, μ, and β represent the frequency ratio, damping ratio, mass ratio, and inertance ratio, respectively.

7. MODELING OF THE 9-STORY STEEL MOMENT-RESISTING FRAME

The benchmark structural model employed in this investigation consists of a 9-story steel moment-resisting frame featuring five bays. The ground-story height is 5.49 *m*, while the remaining stories each have a height of 3.96 *m*. Detailed specifications for this frame are documented in reference [45]. The structure possesses a total mass of 9.00×10^6 *kg*, and the bay width is uniformly set at 9.15 *m*.

The fundamental periods of vibration for the first three modes are 2.27 *s*, 0.85 *s*, and 0.49 *s*, respectively. A modal damping ratio of 2% is assumed throughout the analyses. The yield strength of the column material is 345 *MPa*, while that of the beams is 248 *MPa*. This baseline information underpins all subsequent dynamic analyses and seismic performance evaluations. The numerical model was developed within the OpenSees framework using a concentrated plasticity formulation. To capture the nonlinear response at beam-column joints, zero-length rotational springs with nonlinear characteristics were incorporated, representing the lumped plasticity behavior. The beam and column elements themselves were assigned elastic material properties. The nonlinear cyclic response of these spring elements was governed by the modified Ibarra-Medina-Krawinkler hysteretic model [46].

8. ARTIFICIAL GROUND MOTION

A synthetic earthquake acceleration time history was also employed to excite the base of the structure, generated according to the following formulation:

$$S_{Kanai-Tajimi}(\omega) = S_0 \left[\frac{\omega_g^4 + (2\times\omega_g\times\xi_g\times\omega)^2}{(\omega^2-\omega_g^2)^2 + (2\times\omega_g\times\xi_g\times\omega)^2} \right]$$
$$S_0 = \frac{0/03\times\xi_g}{\pi\times\omega_g\times(4\times\xi_g^2+1)} \tag{19}$$

As defined in Equation (19), S_0 denotes the intensity of the Power Spectral Density Function (PSDF) [47]. The parameters ω_g and ξ_g in this expression correspond to the natural circular frequency and the damping coefficient of the underlying soil medium, respectively. For the present study, the soil frequency is taken as 25.13 *rad/s* with a damping ratio of 0.8 [48]. A peak ground acceleration (PGA) of 0.8 *g* is applied during the dynamic analysis. Figure (5) illustrates the acceleration time history of the generated artificial earthquake, while Table (3) summarizes its key technical parameters.

Table 3: Some properties of the artificial earthquake.

Earthquake	PGA (m/sec^2)	PGA/PGV ($g.sec/m$)	Strong ground motion duration (*sec*)	Predominant period (*sec*)	Total time duration (*sec*)	Arias Intensity (m/*sec*)
Artificial earthquake	8.024	0.0022	18	0.22	19.89	1499

Subsequently, the 9-story moment frame was subjected to the aforementioned artificial earthquake, and the optimal parameters for the four damper configurations (i.e., PTMDI, TMDI, PTMD, and TMD) were determined with the objective of minimizing the Park-Ang damage index. The optimization aimed to achieve improved seismic performance and to mitigate structural damage under severe shaking.

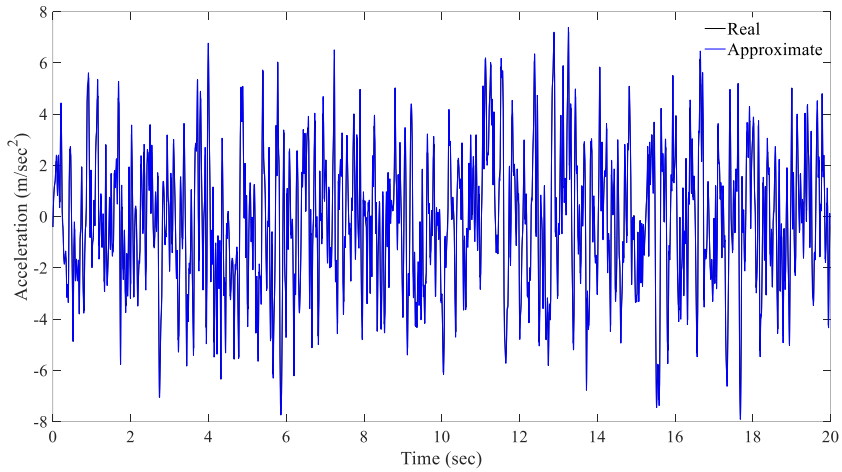

Figure 5. Time history record of the artificial earthquake acceleration.

9. RESULTS AND DISCUSSION

9.1. Comparative Effectiveness of PTMDI, TMDI, PTMD, and TMD in Reducing the Park-Ang Damage Index

The numerical simulations were performed on the 9-story frame under the artificial earthquake excitation, with the optimal design parameters for each of the four damper types identified using the Harris Hawks optimization algorithm. The outcomes indicate that both the PTMDI and TMDI systems provide meaningful reductions in the Park-Ang damage index. The optimization procedure utilized an initial population of 20 candidate groups, from which the most favorable set was selected and subsequently kept consistent throughout all optimization runs for each damper type. This strategy was adopted to ensure that the optimization process began from identical starting points across all cases, thereby eliminating any bias introduced by differing initial conditions and enabling a more reliable comparison of damper performance.

Table 4 reports the computed damage indices for the uncontrolled structure as well as for the structure equipped with each damper type, offering a clear quantitative assessment of the effectiveness of each seismic control strategy.

The results obtained from the numerical simulations indicate that, under optimally tuned conditions, both the PTMDI and TMDI systems exhibit considerable effectiveness in mitigating the Park-Ang damage index, with reductions of 38% and 35%, respectively. In addition, both damper types contribute significantly to the attenuation of roof acceleration responses.

Nevertheless, it is observed that the application of PTMDI and TMDI results in a modest increase in the overall interstory drift of the structure. Importantly, however, this increase remains within the permissible drift limit of 0.025, thereby complying with the prescribed standard thresholds. Meanwhile, although the TMD and PTMD configurations lead to an increase in roof displacement, they still provide a beneficial effect in terms of reducing the Park-Ang damage index.

Table 4: Comparison of the performance of structures controlled with different control systems and the uncontrolled structure.

System	Roof disp. (*m*)	Roof accel. (*g*)	Global drift ratio	Park-Ang damage index	Reduction Percentage (%)			
					Roof disp.	Roof accel.	Global drift ratio	Park-Ang damage index
Uncontrol	0.735	11.82	0.0075	0.452	N/A	N/A	N/A	N/A
Controlled by TMD	0.739	11.65	0.0073	0.439	-0.54	1.49	2.27	4.99
Controlled by TMDI	0.708	10.19	0.0085	0.293	3.61	13.80	-12.34	35.92
Controlled by PTMD	0.740	11.73	0.0072	0.449	-0.67	0.77	4.51	2.78
Controlled by PTMDI	0.703	10.29	0.0141	0.289	4.33	12.99	-86.96	38.13

In addition, Figure 6 provides a comparative summary of interstory drift values for two structural conditions: the uncontrolled configuration and the optimally controlled configurations equipped with various damping systems. This figure facilitates a detailed assessment of how each damper influences relative story displacements, thereby underscoring the contribution of seismic control strategies to enhanced structural performance.

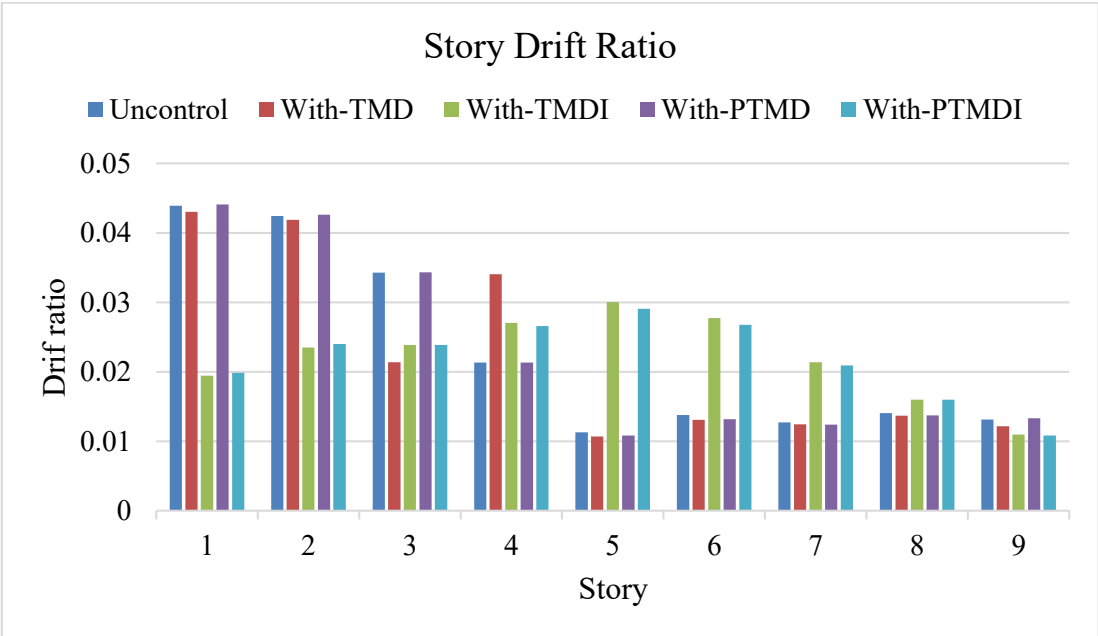

Figure 6: A comparison between the maximum drift stories for the uncontrolled and controlled structures subjected to the artificial earthquake.

Examination of the data in Figure 6 reveals that the PTMDI system exhibits limited effectiveness in reducing drift within the lower stories; however, it proves considerably more capable in mitigating drift at upper levels. Furthermore, Figure 7 illustrates the distribution of

Park-Ang damage index throughout the height of the structure, clearly demonstrating the seismic damage mitigation achieved through the application of the PTMDI system.

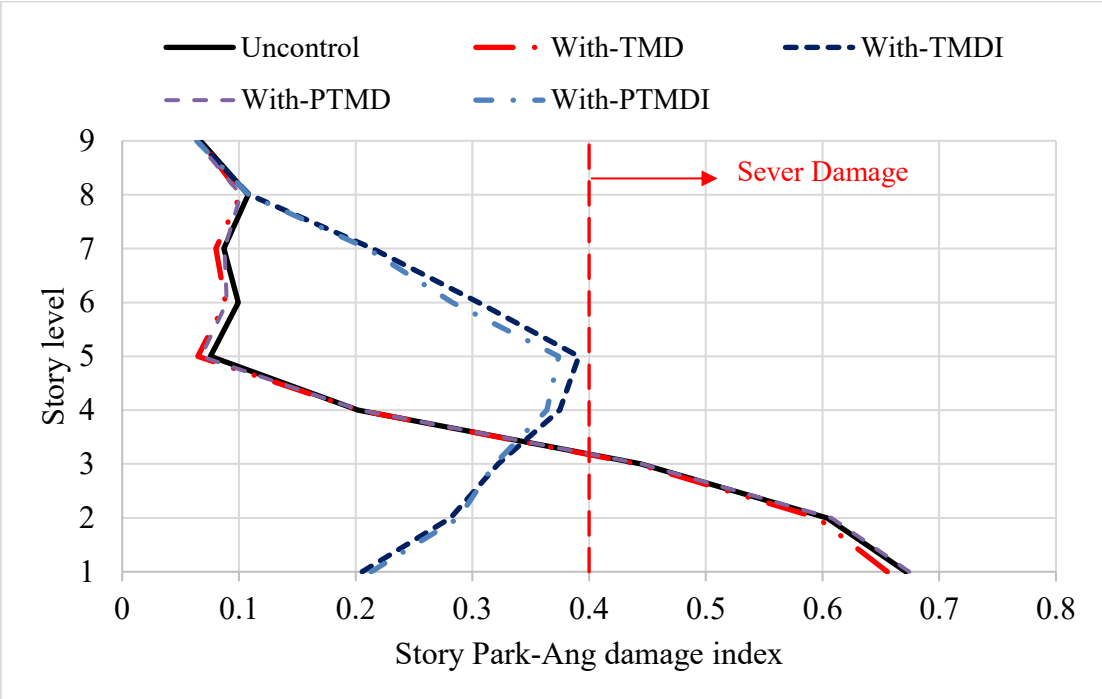

Figure 7: Distribution of the Park-Ang damage index across stories for uncontrolled and controlled structures subjected to the artificial earthquake.

From the trends observed in Figure 6, it is evident that both the PTMDI and TMDI systems fail to deliver substantial drift reduction in the lower portion of the structure. In contrast, at higher elevations, these two systems yield notable drift reductions, indicating their growing effectiveness with increasing story height.

Figure 7 further reveals that the distribution of the story damage index across the building height is considerably more uniform when TMDI or PTMDI systems are employed, in comparison to other control strategies. This uniformity is advantageous, as it prevents the concentration of damage within a single story—particularly critical in lower stories—thereby reducing the risk of progressive collapse.

The optimal parameter values derived for each control system under the artificial earthquake excitation, obtained via the Harris Hawks optimizer, are summarized in Table 5.

Table 5: Optimized control system parameters under artificial seismic excitation.

System	k_T	c_T	m_T	ν	ζ	μ	β	*Stroke (m)*
TMD	7.8462×10^4	9.3542×10^4	7.0991×10^5	1.32	0.1982	0.0105	-	0.4014
TMDI	7.8462×10^4	9.3542×10^4	7.0991×10^5	1.32	0.1982	0.0105	0.5018	0.3373
PTMD	7.6430×10^4	-	5.6612×10^5	1.20	-	0.0102	-	0.6604
PTMDI	7.8462×10^4	-	7.0991×10^5	1.32	-	0.0105	0.5018	0.7098

10. CONCLUSION

In the present study, a novel PTMDI system is proposed, developed by eliminating the viscous damper and incorporating elastoplastic stiffness in its place. The primary aim is to evaluate its seismic performance relative to other vibration control systems (i.e., TMDI, PTMD, and TMD systems). For each system, optimal parameters are identified through minimization of the Park-Ang damage index, thereby maximizing the structure's resistance to seismic loading.

Numerical simulations are conducted on a 9-story moment-resisting frame, modeled using the IMK nonlinear formulation with concentrated plasticity at connections, implemented within the OpenSees environment. The Harris Hawks optimizer is selected here, and to enhance the computational accuracy, a coupled MATLAB-OpenSees framework is employed, with a fixed population size and 900 iterations per optimization run.

The numerical outcomes demonstrate that the PTMDI system surpasses the alternative control methods, achieving up to a 38% reduction in the structural damage index—a result attributed to the replacement of linear stiffness with elastoplastic behavior. This performance advantage underscores its practical potential.

Moreover, the PTMDI system achieves up to 50% damage reduction in the lower stories—the regions most susceptible to severe damage and critical to overall stability. This substantial decrease in localized damage significantly lowers the probability of global collapse.

Collectively, the numerical evidence confirms that the proposed PTMDI system offers substantial capabilities in reducing roof displacement, roof acceleration, and the Park-Ang damage index across individual stories and the entire structure, positioning it as a promising solution for seismic performance enhancement.

ACKNOWLEDGMENT

The authors would like to thank the General Directorate of School Renovation of Kerman Province (Kerman, Iran) for their collaboration in providing the necessary research funds for this paper, which was of great help in completing this work.

REFERENCE

1. Ormondroyd J, Hartog JPD. *The Theory of Dynamic Vibration Absorber*. 1928.
2. Brock J. A note on the damped vibration absorber. *J Appl Mech*. 1946;**13**(4):A284.
3. Kaveh A, Javadi SM, Moghanni RM. Optimal structural control of tall buildings using tuned mass dampers via chaotic optimization algorithm. *Struct*. 2020;**28**:2704–13.
4. Kaveh A, Ardebili SR. A comparative study of the optimum tuned mass damper for high-rise structures considering soil–structure interaction. *Period Polytech Civ Eng*. 2021;**65**(4):1036–49.
5. Kaveh A, Fahimi Farzam M, Hojat Jalali H. Statistical seismic performance assessment of tuned mass damper inerter. *Struct Control Health Monit*. 2020;**27**(10).

6. Kaveh A, Pirgholizadeh S, Khadem Hosseini O. Semi-active tuned mass damper performance with optimized fuzzy controller using CSS algorithm. *Asian J Civ Eng*. 2015;**16**(5):587–606.
7. Rana R, Soong TT. Parametric study and simplified design of tuned mass dampers. *Eng Struct*. 1998;**20**(3):193–204.
8. Hartog JPD. *Mechanical Vibrations*. McGraw-Hill; 1974.
9. Asami T, Nishihara O, Baz AM. Analytical solutions to H∞ and H2 optimization of dynamic vibration absorbers attached to damped linear systems. *J Vib Acoust*. 2002;**124**(2):284–95.
10. Moutinho C. An alternative methodology for designing tuned mass dampers to reduce seismic vibrations in building structures. *Earthq Eng Struct Dyn*. 2012;**41**(14):2059–73.
11. Kamgar R, Khatibinia M. Multi-objective optimization design of tuned mass damper system subjected to critical excitation (In Persian). *Mod Civ Eng J*. 2017;**17**(4):153–64.
12. Khatibinia M, Gholami H, Kamgar R. Optimal design of tuned mass dampers subjected to continuous stationary critical excitation. *Int J Dyn Control*. 2018;**6**:1094–1104.
13. Smith MC. Synthesis of mechanical networks: the inerter. *IEEE Trans Autom Control*. 2002.
14. Nakamura Y, et al. Seismic response control using electromagnetic inertial mass dampers. *Earthq Eng Struct Dyn*. 2014;**43**(4):507–27.
15. Soong TT, Dargush GF. *Passive Energy Dissipation Systems in Structural Engineering*. 1997;**34**:65–66.
16. Kamgar R, Khatibinia M, Khatibinia M. Optimization criteria for design of tuned mass dampers including soil–structure interaction effect. *Int J Optim Civ Eng*. 2019;**9**(2):213–32.
17. Gholizadeh S, Shahrezaei AM. Optimal placement of steel plate shear walls for steel frames by BAT algorithm. *Struct Des Tall Spec Build*. 2015;**24**(1):1–18.
18. Kaveh A, Kalateh-Ahani M, Fahimi-Farzam M. Constructability optimal design of reinforced concrete retaining walls using a multi-objective genetic algorithm. *Struct Eng Mech*. 2013;**47**(2):227–45.
19. Kaveh A, Fahimi Farzam M, Maroofiaz R. Comparing H2 and H∞ algorithms for optimum design of tuned mass dampers under near-fault and far-fault earthquake motions. *Period Polytech Civ Eng*. 2020;**64**(3):904–16.
20. Bilondi MRS, Yazdani H, Khatibinia M. Seismic energy dissipation-based optimum design of tuned mass dampers. *Struct Multidiscip Optim*. 2018;**58**:2517–53.
21. Bakre SV, Jangid RS. Optimum parameters of tuned mass damper for damped main system. *Struct Control Health Monit*. 2007;**14**(3):448–70.
22. Bekdaş G, Nigdeli SM. Estimating optimum parameters of tuned mass dampers using harmony search. *Eng Struct*. 2011;**33**(9):2716–23.
23. Lu Z, Li K, Ouyang Y, Shan J. Performance-based optimal design of tuned impact damper for seismically excited nonlinear building. *Eng Struct*. 2018;**160**:314–27.
24. Lazar IF, Neild SA, Wagg DJ. Using an inerter-based device for structural vibration suppression. *Earthq Eng Struct Dyn*. 2014;**43**(8):1129–47.
25. Hu Y, Chen MZQ. Performance evaluation for inerter-based dynamic vibration absorbers. *Int J Mech Sci*. 2015;**99**:297–307.

26. Giuliano F. Note on the paper "Optimum parameters of tuned liquid column–gas damper…" *Struct Control Health Monit*. 2013;**20**(5):852–52.
27. Chen G, Wu J. Optimal placement of multiple tuned mass dampers for seismic structures. *J Struct Eng*. 2001;**127**(9):1054–62.
28. Pinkaew T, Lukkunaprasit P, Chatupote P. Seismic effectiveness of tuned mass dampers for damage reduction of structures. *Eng Struct*. 2003;**25**(1):39–46.
29. Nakamura Y, et al. Seismic response control using electromagnetic inertial mass dampers. *Earthq Eng Struct Dyn*. 2014;**43**(4):507–27.
30. Marian L, Giaralis A. Optimal design of a novel tuned mass-damper–inerter (TMDI) passive vibration control configuration for stochastically support-excited structural systems. *Probabilistic Eng Mech*. 2014;**38**:156–64.
31. Brzeski P, Pavlovskaia PE, Kapitaniak T, Perlikowski P. The application of inerter in tuned mass absorber. *Int J Nonlinear Mech*. 2015;**70**:20–29.
32. Zhang SY, Jiang JZ, Neild S. Optimal configurations for a linear vibration suppression device in a multi-storey building. *Struct Control Health Monit*. 2017;**24**(3):e1887.
33. Jaiswal OR, Chaudhari J, Madankar NH. Elasto-plastic tuned mass damper for controlling seismic response of structures. *World Conf Earthq Eng*. 2008.
34. Heidari AA, Mirjalili S, Faris H, Aljarah I, Mafarja M, Chen H. Harris hawks optimization: algorithm and applications. *Future Gener Comput Syst*. 2019;**97**:849–72.
35. Alsattar HA, Zaidan AA, Zaidan BB. Novel meta-heuristic bald eagle search optimisation algorithm. *Artif Intell Rev*. 2020;**53**:2237–64.
36. Chopra AK. *Dynamics of Structure*. Prentice Hall of India; 2006.
37. FEMA-356. *Standard and Commentary for the Seismic Rehabilitation of Buildings*. 2000.
38. Park YJ, Ang AHS. Mechanistic seismic damage model for reinforced concrete. *J Struct Eng*. 1985;**111**(4):722–39.
39. Park YJ, Ang AHS, Wen YK. Damage-limiting aseismic design of buildings. *Earthq Spectra*. 1987;**3**(1):1–26.
40. Kunnath SK, Reinhorn AM, Park YJ. Analytical modeling of inelastic seismic response of RC structures. *J Struct Eng*. 1990;**116**(4):996–1017.
41. Kunnath SK, Reinhorn AM, Lobo RF. *IDARC Version 3: A Program for the Inelastic Damage Analysis of Reinforced Concrete Structures*. Nat Center Earthquake Eng Res; 1992.
42. De Domenico D, Ricciardi G. Optimal design and seismic performance of tuned mass damper inerter (TMDI) for structures with nonlinear base isolation systems. *Earthq Eng Struct Dyn*. 2018;**47**(12):2539–60.
43. Lignos DG, Krawinkler H. Deterioration modeling of steel components in support of collapse prediction of steel moment frames under earthquake loading. *J Struct Eng*. 2011;**137**(11):1291–302.
44. FEMA 356. *NEHRP Recommended Provisions for Seismic Regulations for New Buildings and Other Structures*. Building Seismic Safety Council; 2000:159–60.

45. ASCE/SEI. *Seismic Rehabilitation of Existing Buildings*. American Society of Civil Engineers; 2007:120.
46. Ohtori Y, Christenson RE, Spencer BF, Dyke SJ. Benchmark control problems for seismically excited nonlinear buildings. *J Eng Mech*. 2004;**130**(4):366–85.
47. Kanai K. A statistical method of determining the maximum response of a building structure during an earthquake. *Proc 2nd World Conf Earthq Eng*. 1960.
48. Wu J, Chen G, Lou M. Seismic effectiveness of tuned mass dampers considering soil–structure interaction. *Earthq Eng Struct Dyn*. 1999;**28**(11):1219–23.